2

Conf-930241--2

UCRL-JC-110987
PREPRINT

Dynamic Characterization of a Lightweight, Highly Maneuverable Spacecraft Using Modal and Finite Element Analyses

Patricia A. Manning, R. Bradley Burdick, Thomas G. Woehrle

This paper was prepared for submittal to the
International Modal Analysis Conference
Kissimmee, Florida
February 1-4, 1993

November 1992

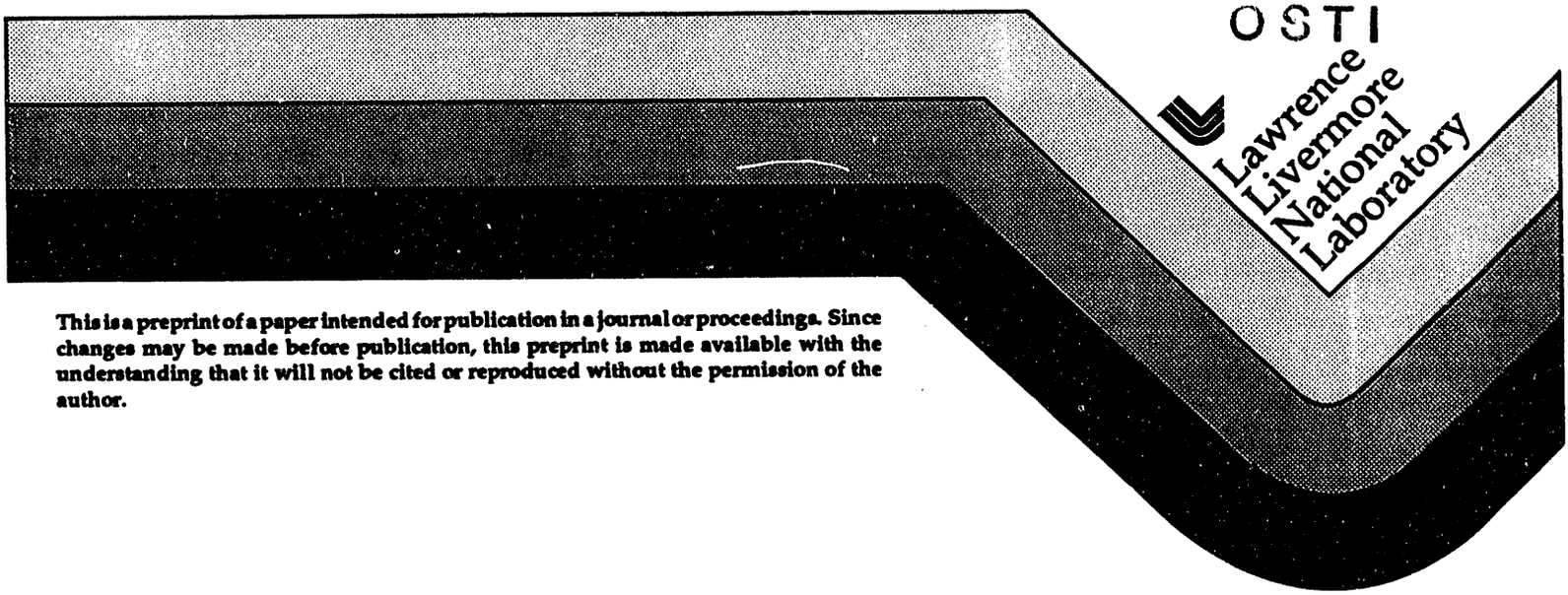

DYNAMIC CHARACTERIZATION OF A LIGHTWEIGHT, HIGHLY MANEUVERABLE SPACECRAFT USING MODAL AND FINITE ELEMENT ANALYSES *

Patricia A. Manning, Engineer
R. Bradley Burdick, Section Leader
Thomas G. Woehrle, Technical Associate
Lawrence Livermore National Laboratory
Livermore, CA 94550, USA

Abstract

The Lawrence Livermore National Laboratory is engaged in a technology development project which includes designing a lightweight, autonomous, highly maneuverable space vehicle, commonly referred to as a probe. The current probe design includes a guidance and control system that requires complete information on the dynamic response of the probe during operation. A finite element model of the probe was constructed to provide analytical information on the dynamic response to specific operational inputs. In order to verify the assumptions made in the model, a mass mock-up of the probe was constructed at LLNL and an experimental modal survey was performed to determine the frequencies, damping values and deflection shapes for each natural mode of the mock-up. The experimental modal parameters were compared with the parameters obtained through modal analysis of the finite element model to provide a measure of the correlation between the model and the actual structure. This report describes the experimental modal testing and analysis of the mass mock-up and compares the experimental results with the finite element results.

Nomenclature

$\gamma 2$	Coherence Function
$G_{AB}(f)$	Cross Spectrum between points A and B
$G_{AA}(f)$	Auto Spectrum at point A
$G_{BB}(f)$	Auto Spectrum at point B
$X_j(\omega)$	Fourier Transform of response vibrations
$F_i(\omega)$	Fourier Transform of force input
$H_{ij}(\omega)$	Frequency Response Function between points i and j

Introduction

The Lawrence Livermore National Laboratory is engaged in a technology development project which includes designing a lightweight, autonomous, highly maneuverable space vehicle, commonly referred to as a probe. The current probe design includes a guidance and control system that requires complete information on the dynamic response of the probe during operation. A finite element model of the probe was constructed to provide detailed information on the dynamic response to specific operational inputs. The finite element model (FEM) was based on assumptions about various parameters of each element of the structure, such as the stiffness, damping and connection properties of the bolted, screwed and welded joints in the probe.

The only way to verify the assumptions made by the FEM was through comparison with actual response data. A mass mock-up of the probe design was constructed at LLNL for experimental modal testing. A modal survey of the mass mock-up was performed and modal analysis of the experimental data was used to determine the frequencies, damping values and deflection shapes for each natural mode of the mock-up. At the same time, the finite element model was modified to reflect a few simplifications inherent in the mass mock-up. The experimental modal parameters were compared with the parameters obtained through the modified finite element model to provide a measure of the correlation between the model and the actual mock-up structure. Once the FEM of the mass mock-up satisfactorily predicts the actual dynamic response of the mass mock-up, it can be expanded to represent the current probe design. The expanded FEM can then be used with significantly improved confidence to evaluate structural integrity during launch and to predict deflections under operational loading.

This report details the experimental modal testing and analysis of the mass mock-up. The mock-up was tested with depleted fuel tanks. The natural frequencies, damping values and associated deflection shapes of the mass mock-up were determined for all modes below 140 Hertz. The measured frequencies and shapes were compared to the analytic modes predicted by the finite element model. In addition, modes which caused misalignment between the critical sensors of the control system were identified.

Experimental Modal Analysis of the Mass Mock-up

Three complete modal surveys were performed on the mass mock-up. The first (Test A) was a preliminary survey with a greatly reduced set of measurement locations. Measurements were taken in one direction only. The purpose of this test was to obtain an initial

indication of the mock-up's linearity and the likelihood of gaining meaningful data from an extensive test. The results of Test A showed a linear response in the range of our excitations. Also, the presence of global mode shapes was indicated. This was an important result of the preliminary test, since the vibration response of a structure as complicated as the mock-up is sometimes dominated by local effects. Loose joints and many small sub-components are the most common cause of this type of behavior.

The second survey (Test B) was more detailed. The results of the preliminary test were used to guide selection of measurement locations for this test. It was designed to provide complete information on the natural dynamic response of the mass mock-up. After all measurements were completed, the forward (+x) box of the mass mock-up was disassembled to fix a rattle discovered during the latter part of the survey. (The rattle was not fixed during the test because of the possible change in dynamic response due to changes in bolt torques and cable attachment locations.)

After the mock-up was reassembled, it was decided that measurement locations should be added to the modal model to provide greater detail on the motion of the IMU and the LIDAR and to add the four main thruster cups to the grid. The set-up for Test B was duplicated and measurements were taken to check repeatability of the original measurements. Due to changes in the structure caused by disassembly, the original measurements could not be repeated. Changes in the transfer functions included frequency shifts and differences in peak magnitudes. Because of these differences, the new data, although equally valid, could not be analyzed in the same group as the old data.

Since new measurements could not be added to the data for Test B, it was decided that a third survey (Test C) was necessary. The grid of measurement locations was modified to include more points on the sensors and the thruster cups. Test C was completed and the results are listed and compared to the Test B results later in this report.

Test Set-up

The test set-up for all three tests was identical except for the grid of measurement locations. The mass mock-up was mounted in an approximately free-free condition and excited with an electromagnetic shaker with a 0 - 400 Hertz random input. Lightweight accelerometers were used to measure the response. Before the testing began, a brief linearity check was performed and all equipment in the measurement chain was calibrated.

Mounting

Since the intended operational environment of the probe is free space, the mass mock-up was mounted with as little constraint to its movement as possible. A free-free condition was approximated by suspending the mock-up from a small crane using soft bungee cords. The mock-up was suspended from two L-brackets bolted into pre-existing holes in the top edge of each bulkhead. (See Figure 1.) The natural bouncing resonance of the mock-up in this configuration (approximately 2 Hertz) was much lower than the lowest mock-up resonance, so that modes of the mounting crane and bungee cords did not confuse the analysis of the main structural modes of the mock-up.

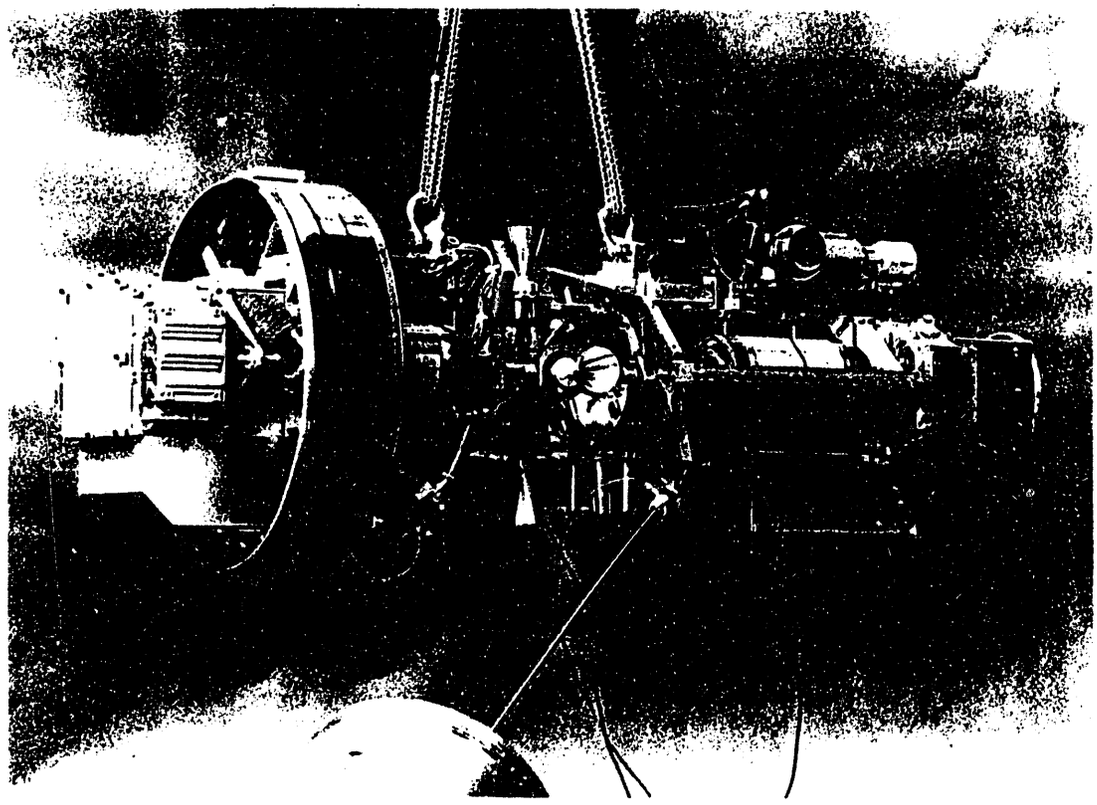

Figure 1: Test Set-up

Excitation

An electro-magnetic shaker was used to excite the mock-up with a well defined random input force. A two foot stinger (or push\pull rod) was attached to the lower corner of one of the bulkheads through a pre-existing hole. The other end of the stinger was attached to the head of the shaker. (See Figure 1.) A force gage was mounted between the stinger and the corner of the bulkhead to measure the input force. The force gage was mounted in line with the axis of the stinger. The lateral flexibility of the stinger assured that force could only be transmitted along the axis of the stinger, so that all of the input to the mock-up was measured by the force gage. This is an important aspect of the test set-up since the accuracy of the frequency response functions depends upon the accuracy and completeness of the input force measurement.

The frequency range of the modal survey was based on the initial predictions of the finite element model. The first six natural frequencies of the mock-up were predicted to be between 84 and 128 Hertz. A spectrum analyzer with signal generation capabilities was used to generate a 0 - 400 Hertz random voltage signal which was fed through a power amplifier into the shaker. This frequency range was chosen to excite at least the first six resonances of the mock-up so that a solid comparison could be made with the finite element model. The input force level in the time domain was 1.2 lbf RMS. Input acceleration level (measured with an accelerometer mounted on the force gage) was 0.94 g's RMS in the time domain. The excitation was applied at a skew angle (approximately 45°-45°-45°) in order to excite all modes of the structure. (See Figure 1.)

Measurement Chain

Piezoelectric accelerometers were used to measure the acceleration response to the shaker input. The accelerometers were mounted onto the mock-up using beeswax. Each accelerometer weighed 7 grams. Only one accelerometer at a time was mounted at any given location so that the added mass was negligible compared to the participating mass at each location. Voltage signals from the accelerometers and the force gage were fed through a constant current source into a spectrum analyzer for processing and storage.

Linearity

After the equipment was completely set up, a brief test was performed to check the linearity of the mock-up's response in the neighborhood of the excitation level. Measurements for the linearity check were taken in three orthogonal directions at four representative locations. Data was collected for three excitation levels: 0.38 lbf, 1.29 lbf, and 3.47 lbf RMS in the time domain. Overlays of the three measurements for each location and direction show good linearity (within 25% for amplitude and 1% for frequency) for most of the modes between 70 Hertz and 140 Hertz. The peaks at 76 and 86 Hertz, however, show slight nonlinearity, changing in amplitude as much as 50% and in frequency as much as 2.3%. Changes of this magnitude in frequencies and amplitudes were not expected to significantly effect the modal analysis of the mock-up.

Calibration

All equipment used in the modal survey was calibrated to insure accurate data. The accelerometers and the force gage were calibrated before and after the test. The sensitivities changed by less than 4% during the test.

In addition to individual transducer calibrations, a free-mass calibration was used to check the system as a whole. The acceleration and phase of a known mass were measured and compared to the measured input force. The weight of the known mass was 56.5 pounds. The calculated weight (force / acceleration) was 58.6 pounds.

Data Collection

In order to generate a complete set of frequency response functions for the mass mock-up, response accelerations were measured at a grid of output locations spread out around the main structural elements of the mock-up. The grid of measurement locations was chosen differently for each of the three modal surveys, depending on the goals of the particular survey. At each measurement location, the auto spectra and the cross spectra for each measurement direction were collected and saved for future analysis. For each measurement, the coherence function was calculated and watched as an on-line check of the integrity of the data.

Measurement Locations

Measurement locations for each of the three modal surveys were chosen such that the important global motions of the mass mock-up and some of its subcomponents were captured. Care was taken to choose locations that would exhibit global motions so that local effects would be minimized. Special attention was paid to two sensors which are considered critical to the operation of the probe's control system. The Laser Imaging Radar (LIDAR) and the Inertial Measurement Unit (IMU) were included in the grid of measurement locations so that any relative misalignment between them could be identified.

The main structural elements of the mass mock-up which were included in the measurement grids are:

- the **two boxes** housing the interior fuel tanks and supporting the various measurement and control equipment,
- the **two bulkheads** supporting the fuel tanks and the boxes,
- the **bridge** connecting the bulkheads (and boxes) and supporting the four main thrusters,
- the **circular antenna** attached to the -X box,*
- the **LIDAR truss structure** attached to the front end of the +X box, and
- the **IMU** attached to the bottom of the +X box and covered with a thin-walled box.

* (See Figure 2 for axes of orientation.)

TEST A For the preliminary modal survey (Test A), a minimal set of measurement locations was chosen. Measurements were taken in only one direction at 22 locations. The measurement grid is shown in Figure 2. It includes eight locations on each box and one location on each inner fuel tank, four locations on the antenna, two locations on each bulkhead (modeling the bulkheads as diagonal lines), four locations on the cover of the IMU and one location on the tip of the LIDAR truss structure. The two boxes appear to be unconnected in the model because no measurements were taken on the bridge, but they were treated as one (connected) structure in the analysis.

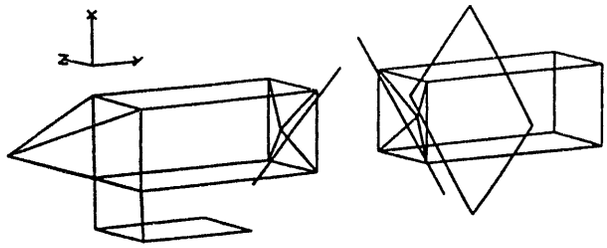

Figure 2: Measurement Grid for the Preliminary Test

TEST B For Test B, a more refined grid of measurement locations was used. Measurements were taken in three orthogonal directions at 100 locations. The measurement grid used for Test B is shown in Figure 3. The full shapes of the antenna, the bulkheads, and the bridge are shown in this model.

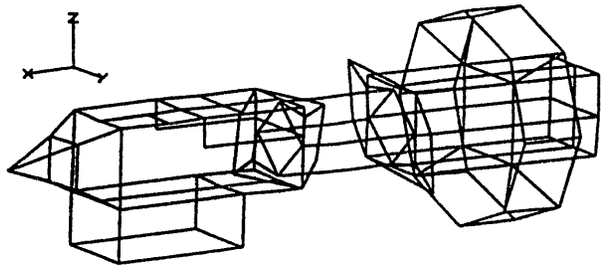

Figure 3: Measurement Grid for Test B

TEST C The grid for Test B was modified to reflect changes in the desired detail on the LIDAR, IMU, thruster cups, antenna and bulkheads for Test C. Measurement locations were added to the LIDAR to enable identification of 1) its bending modes and 2) the motion of the LIDAR end plate. Since motion of the sensors mounted on the base plate of the IMU are of primary concern, measurement locations were also added on the base plate of the IMU. Measurements were still taken on the thin IMU cover, although they are not indicative of the motion of the IMU sensors. Measurement locations on the bulkheads and the antenna were reduced in number since Test B provided ample information on the modal characteristics of these components. Measurements were taken in three orthogonal directions at 78 locations. The measurement grid for Test C is shown in Figure 4.

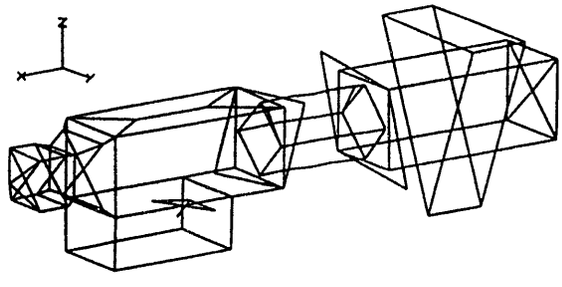

Figure 4: Measurement Grid for Test C

Measurement Parameters

For each measurement location on the grid, data was collected in three orthogonal directions (except in the preliminary test). The input auto-power-spectrum, output auto-power-spectrum and cross-power-spectra were generated and saved for each direction. Measurements were taken with a frequency bandwidth of 0 - 312 Hertz, and a Hanning window was applied to the data to eliminate leakage of discrete frequency components into sidebands. Due to the density of modes in the bandwidth of interest, high resolution measurements were made (2000 frequency lines, 0.16 Hertz resolution).

Coherence Monitoring

During the test, the coherence functions were monitored as an on-line check of the quality of the data. Theoretically, the coherence function gives a measure of the degree of linear dependence between two signals as a function of frequency. The coherence drops below its perfect value of unity when there is noise in the system or when there is a non-linear relationship between the two measured signals.

The coherence function is calculated from the two auto spectra and the cross spectrum by the equation:

$$\gamma^2(f) = \frac{|G_{AB}(f)|^2}{G_{AA}(f) \cdot G_{BB}(f)} \qquad (1)$$

where: $\gamma^2(f)$ is the coherence function, $G_{AB}(f)$ is the cross spectrum between points A and B, and $G_{AA}(f)$ and $G_{BB}(f)$ are the auto spectra at points A and B respectively.

For practical purposes, the coherence function is an excellent tool for identifying problems in the measurements. Loose or damaged cables and accelerometers, loose screws on the mock-up, and excessive noise in the area all degrade the quality of the data and in some cases invalidate it. Each of these conditions show up as a drop in coherence. In addition, improper functioning of the measurement equipment can sometimes be seen as a drop in the coherence. Data integrity was maintained during testing by correcting problems as they occurred.

Results

The experimental modal testing and analysis of the mass mock-up was completed. Frequency, damping and mode shape values were extracted from each frequency response function for all modes below 140 Hertz for Tests B and C. Global modal parameters were determined for each mode. The modal parameters from the two tests were compared and consolidated and a master list of observed modes was created. Modes which caused misalignment between the two critical sensors of the control system (the IMU and the LIDAR) were identified using the animated mode shapes. Finally, the master list of observed modes was compared to the list of modes predicted by the finite element model.

Comparison of Data from Tests B and C

Frequencies and mode shape descriptions for every mode evaluated in Test B and Test C are shown in Appendix A. Some differences can be seen between the Test B data and the Test C data. In some cases, the frequencies associated with a particular mode shape are different. The frequency differences represent changes in the structural response, probably resulting from disassembly of the +X box between Test B and Test C. Small differences in the torque on the screws and the attachment of the cable bundle after reassembly could

cause some of these changes. In other cases, mode shapes appear in one set of test data but not in the other. There are two reasons for the apparent absence of these modes. First, some of the modes which were not important to the goals of the project (such as antenna modes) were not fitted in Test C. Second, some of the modes were either not excited or not present in one or the other of the tests. This change in modal response can probably be attributed to changes in the structure itself during disassembly.

Although there were small differences, the general grouping and ordering of modes was the same for Tests B and C. Therefore, the results of the two tests were consolidated into a single set of 'observed modes' for use in comparisons to the finite element model.

Observed Modes

A consolidated list of observed modes from Tests B and C is shown in Table 1. The table lists only the modes considered important to the goals of this project. Three types of modes are listed; torsion and bending modes of the bridge, bending modes of the LIDAR, and a box panel mode. The torsion and bending modes of the bridge and the panel mode are important in the verification of the finite element model. As the lowest modes of the main box, bulkhead and bridge structure, these modes will cause the largest displacements of the IMU and the LIDAR. This makes them important to the operation of the control system as well.

The bending modes of the LIDAR are also important to the operation of the control system. These modes will cause relative displacement between the IMU and the LIDAR, causing gross errors in the response of the control system.

All of these modes are listed in Table 1. Modes which were observed to cause misalignment between the IMU and the LIDAR are identified by a check mark in the table. Since multiple torsion and bending modes are listed, it should be noted that, while each of the modes are dominated by the listed shape description, they differ in the participation of sub-components such as the antenna and various small components. However, motions of the IMU and LIDAR which occur along with one of the other listed modes are listed separately in the table.

Deflection shapes for a representative group of these modes are shown in Appendix D. These mode shapes were also videotaped from the computer screen to more clearly document the identified motion. The animated mode shapes are best used as indicators of the global motion associated with each resonance. They show the relative displacements of the various measurement locations for each mode, but do not indicate absolute displacements.

Comparison of FEM Predictions with Observed Modes

A detailed finite element model of the mass mock-up was created using an internally-written finite element analysis code. In the model, the bridge, bulkheads, boxes and major components and sensors were discretely modeled with solid, beam and shell elements. The model consisted of 6265 nodes with 37,518 active degrees of freedom. The propulsion system, wire harness, static balances and miscellaneous hardware were modeled with lumped masses. The weight of the analytical model (with no static balances and empty fuel tanks) was very close to the actual weight of the mass mock-up.

*Table 1: Summary of Observed Modes**

	Frequency	Damping	Misalignment between LIDAR and IMU
Bridge Torsion	72 Hertz 76 Hertz 82 Hertz 86 Hertz 93 Hertz	1.2% crit. 2.1% crit. 0.9% crit. 2.9% crit. (Note A)	
Bridge Bending about Z axis	86 Hertz 93 Hertz 123 Hertz	2.9% crit. (Note A) 1.0% crit.	
Bridge Bending about Y axis	100 Hertz 130 Hertz	1.9% crit. 1.8% crit.	
Bridge Bending about 45°	107 Hertz 119 Hertz	1.3% crit. 0.6% crit.	
LIDAR Bending about Y axis	104 Hertz	2.1% crit.	✓
LIDAR Bending about Z axis	107 Hertz	1.4% crit.	✓
LIDAR Bending about 45°	123 Hertz 128 Hertz	1.3% crit. 3.1% crit.	✓ ✓
Z Panel Mode	135 Hertz	2.1% crit.	

* (These modes are dominated by the listed mode shapes, differing only in the participation of subcomponents such as the antenna and other smaller sensors.)

NOTE A: The measured damping value for the mode at 93 Hertz is invalid due to a stinger resonance at the same frequency.

A comparison of the experimentally determined modes and the modes predicted by the finite element model is shown in Table 2. The table contains a description of each observed modal response shape and the associated frequencies of the measured and predicted modes. Some of the measured modal frequencies are listed twice in the table because the mode shapes associated with them exhibited two distinct modal response shapes. (For example, the mode at 86 Hertz exhibited both bridge torsion and bridge bending about the Z axis, so it is listed twice.)

The correlation between the predictions of the finite element model and the measured modes is quite good for the bridge bending and torsion modes. The FEM frequencies are within 15% of the *lowest* measured frequency in each modal response group, and they are within 10% of the *average* of the measured frequencies in each group. The antenna mode and the panel mode are not as closely predicted. The panel mode will affect the

readouts of any sensors mounted on the +Z panel and should be matched more closely by the FEM if these sensors are important to the analysis. The antenna mode is not as important since it does not directly affect any of the probe's sensors.

Of particular concern is the absence of the 45° bridge bending modes in the finite element model. These modes will significantly affect all sensors on the probe and should be predicted by the FEM. The absence of the LIDAR modes in the FEM predictions is not of concern since the LIDAR was roughly modeled in the present version of the FEM and on the mass mock-up itself. Future tests are planned to model and test the actual LIDAR structure.

In comparing the experimentally determined modes with the modes predicted by the finite element model it is important to consider a few points. First, the finite element model assumes a free-free boundary condition. This condition was approximated by suspending the mass mock-up from a small crane using very soft bungee cords. However, it is impossible to completely eliminate all boundary conditions induced by the suspension system. In this case there was a slight torque applied around the center of the mock-up. Despite these caveats, considerable success was achieved in matching the predictions of the finite element model with the observed dynamic behavior.

Table 2: Comparison between Measured and Predicted Modes

Predicted Frequency [Hertz]	Description of Modal Response	Measured Frequency [Hertz]
46	antenna rotation about x axis	34
82	bridge torsion	72,76,82, 86,93
96	bridge U bending about z axis	86,93
101	bridge U bending about y axis	100
110	+z panel mode of +x box	135
-	bridge U bending about 45° line	107,119
119	bridge U bending about y axis	130
129	bridge U bending about z axis	123
-	LIDAR modes	104,107,123, 128

Conclusions

Using experimental modal testing and analysis, the modal parameters of the probe mass mock-up were determined for each natural resonance below 140 Hertz. Three complete modal surveys were performed in the process of determining the frequency, damping and mode shape values for each mode. The first was a small-scale preliminary survey which confirmed the linearity of the mock-up's response at the chosen excitation levels, and which positively indicated the feasibility of gaining meaningful results from modal testing. The second was a much more detailed survey designed to provide complete information on the modal properties of the mock-up. The third survey was a modified repeat of the second survey, required due to late changes in the project scope.

The modal parameters determined through the two detailed modal surveys were slightly different due to disassembly of the mock-up between the two tests, but the overall grouping and ordering of modes was the same. The results from the two tests were consolidated and the resulting list of experimentally observed modes was compared to the list of modes calculated by the finite element model. The modal frequencies calculated by the FEM were within 10% of the measured frequencies for the torsional and bending modes of the bridge. Of possible concern, however, were the large differences between the calculated and measured panel mode frequencies, and the absence of the 45° bridge bending modes in the FEM calculations.

Overall, the comparison was quite good between the experimentally observed modal response and the modal response calculated by the finite element model. However, the modal surveys showed a few areas in which the FEM could be improved. Once the FEM satisfactorily predicts the actual measured behavior of the mock-up, it can be used to update the finite element model of the actual probe. The response of the probe to operational inputs such as launch and firing can then be predicted with confidence. These results provide the control system designers with all of the information needed for proper control of the probe.

Future Work

Future work on the mass mock-up will include a repeat modal survey to be performed after the environmental testing at Ball Aerospace in Colorado is finished. This survey is intended to determine whether the dynamic properties of the mass mock-up have been changed by the harsh vibration environment imposed upon it during environmental testing. This will provide valuable information to the system control designers about the stability of the dynamic properties of the system.

*This work was performed under the auspices of the U.S. Department of Energy by Lawrence Livermore National Laboratory under contract No. W-7405-Eng-48.

APPENDIX A: Complete List of Modes for Tests B and C

Mode No.	Frequency (Hz)	First Model	Mode No.	Frequency (Hz)	Second Model
1	33.4	antenna rotation about X axis	1	33.5	antenna rotation about X axis; slight bridge torsion
2	36.5	whole-body rotation about X axis	2	36.4	whole-body rotation about X axis
3	46.3	antenna ovalling and flaring			
4	54.9	antenna shearing in Z and Y direction	3	53.9	antenna ovalling and moving in Y direction
5	59.8	antenna moving along X axis			
6	65.8	antenna rocking-rotation about the X axis			
7	69.5	antenna expanding and contracting in Y			
8	72.2	rocking antenna about the X, whole-body torsion about the X axis			
9	82.7	bridge torsion; antenna in-phase with back box	4	72.3	bridge torsion; antenna in-phase with back box
			5	76.1	same bridge torsion mode as at 72.3 Hz
			6	85.9	bridge torsion, bridge U-bending about the Z axis
10	91.7	bridge U-bending about Z axis	7	91.9	bridge U-bending about the Z axis, torsion
			8	93.0	bridge U-bending about the Z axis, torsion
11	100.1	bridge U-bending about the Y axis	9	103.8	bridge U-bending about the Y axis, LIDAR additional bending about the Y axis, inner fuel tank in back box shifting back and forth in X
			10	107.4	bridge U-bending about the Y and Z axes, LIDAR bending about the Z axis
12	119.4	bridge U-bending about the Z axis			
13	122.3	bridge U-bending about the Y and Z axes	11	123.3	bridge U-bending about the Z axis, LIDAR bending about the Y axis, less about the Z, possible +Z panel mode
			12	127.7	LIDAR bending about the Y axis, lesser LIDAR bending about the Z
14	130.4	bridge U-bending about the Yand Z axis	13	129.8	bridge U-bending about Y and Y axis
15	140.2	+Z panel mode on +X box	14	135.3	+Z panel mode on +X box, bridge U-bending about the Z axis
16	148.7	+Z panel mode similar to 140.2 Hz			

APPENDIX B: Representative Mode Shapes

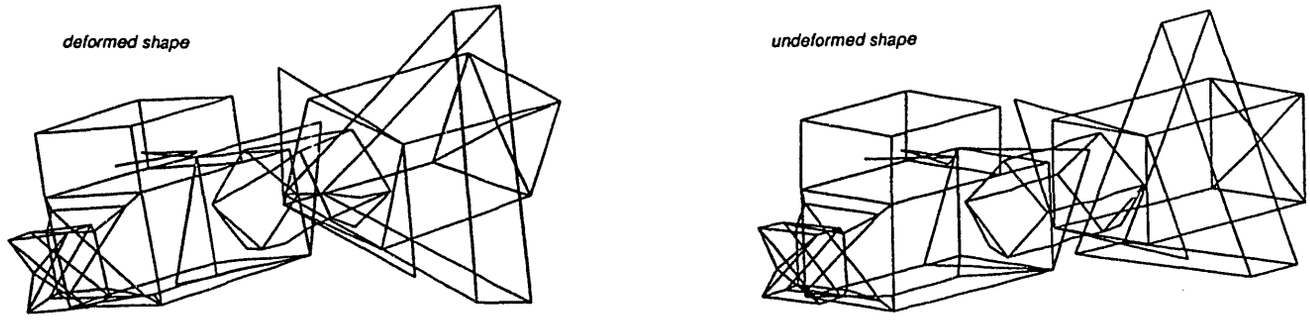

Figure B-1: Bridge Torsion, 72 Hertz

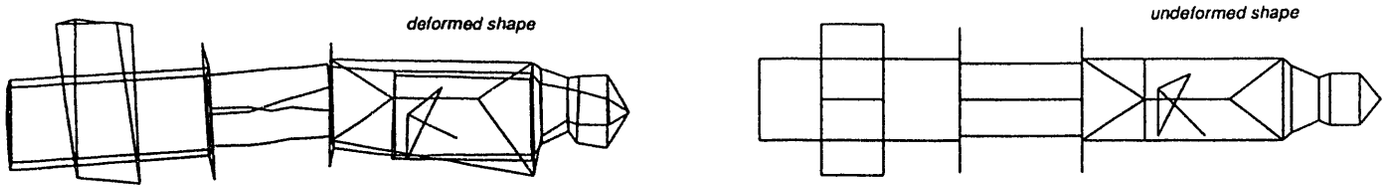

Figure B-2: Bridge Bending about Z Axis, 93 Hertz

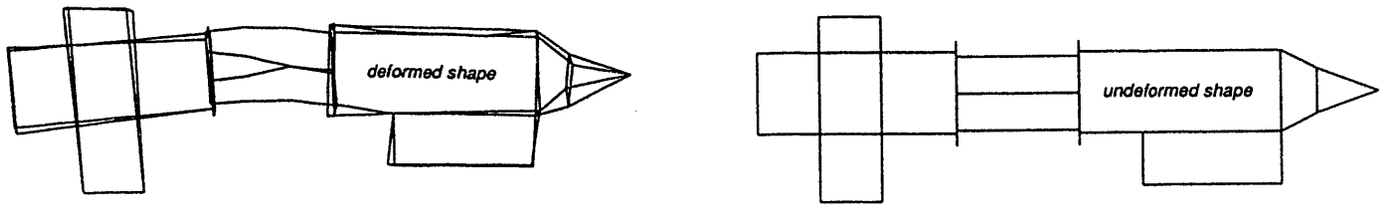

Figure B-3: Bridge Bending about Y Axis, 100 Hertz

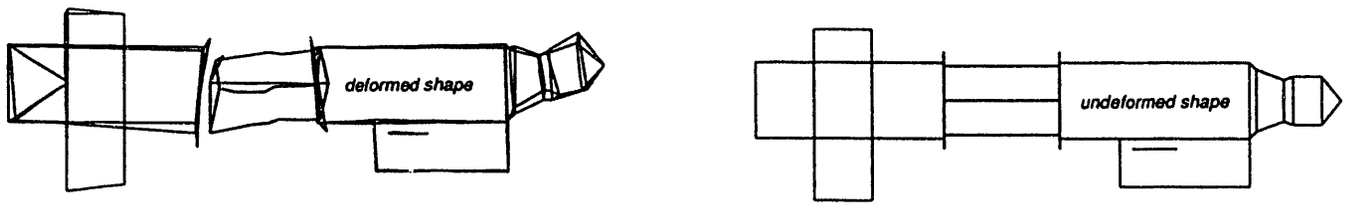

Figure B-4: LIDAR Bending about Y Axis, Fuel Tank Translating along X Axis, 104 Hertz

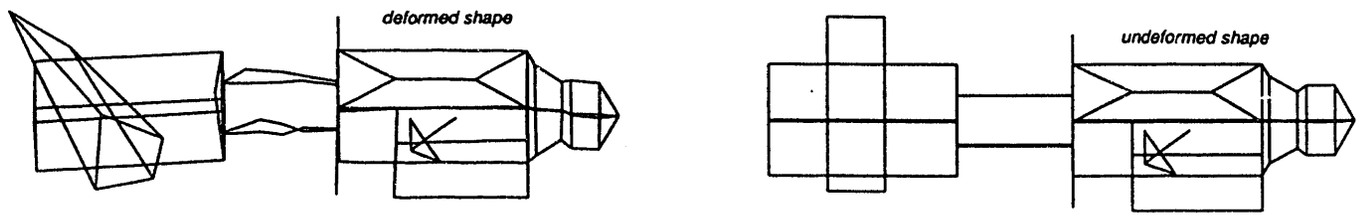

Figure B-5: Bridge Bending about 45 Degree Line, 107 Hertz

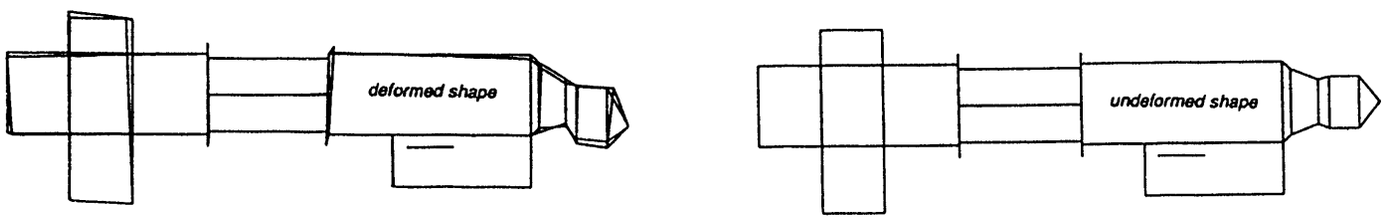

Figure B-6: LIDAR Bending about Y Axis, 128 Hertz

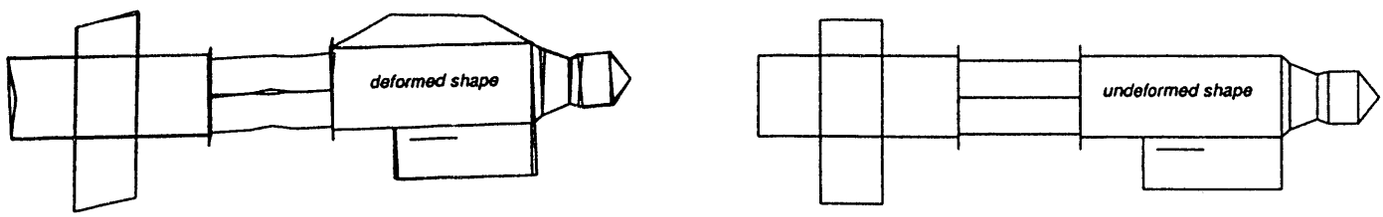

Figure B-7: +Z Panel Mode, 135 Hertz

END

DATE
FILMED
10/6/93